nature communications

Article

https://doi.org/10.1038/s41467-024-51516-1

A seamless auxetic substrate with a negative Poisson's ratio of −1

Received: 11 February 2024

Accepted: 7 August 2024

Published online: 21 August 2024

Check for updates

Yung Lee[1,2,7], Bongkyun Jang[3,7], Hyunggwi Song[1,4], Sumin Kim[1,5], Yong Won Kwon[1,5], Hyun Seok Kang[1,2], Min Seong Kim[4], Inkyu Park[4], Taek-Soo Kim[1,4], Junho Jang[1,2], Jae-Hyun Kim[3], Jang-Ung Park[1,5,6] & Byeong-Soo Bae[1,2]

Auxetic metamaterials are a unique class of materials or structures with a negative Poisson's ratio and a wide array of functionalities. However, their inherent porosity presents challenges in practical applications. Filling the inherent perforations while preserving their unique auxeticity is difficult because it demands the seamless integration of components that have highly distinct mechanical characteristics. Here we introduce a seamless auxetic substrate film capable of achieving a negative Poisson's ratio of −1, the theoretical limit of isotropic materials. This breakthrough is realized by incorporating a highly rigid auxetic structure reinforced by glass-fabric, with surface-flattening soft elastomers. We effectively optimize the mechanical properties of these components by systematic experimental and theoretical investigations into the effects of relative differences in the moduli of the constituents. Using the developed auxetic film we demonstrate an image distortion-free display having 25 PPI resolution of micro-LEDs that is capable of 25% stretching without performance degradation.

Stretchable displays have attracted considerable attention as the cutting edge of future form factor-free screens, because they offer a versatile range of characteristics, space-saving qualities, and design flexibility[1–3]. A pivotal factor in the development of stretchable displays is the substrate's mechanical stability, in particular, its capacity to endure substantial deformation[4]. Prior studies have primarily focused on the stretchability and reliability of the substrate materials, either utilizing intrinsically stretchable elastomers[5,6], or forming extrinsically stretchable structures using inextensible materials such as general kirigami[7,8], serpentine[9–12], and wrinkled structures[2,13–15]. However, most of these approaches often suffer from a critical drawback—image distortion during stretching. Their high positive Poisson's ratio causes contraction in the transverse direction during stretching[12,16,17]. An alternative approach involves the use of the specific forms of kirigami, the auxetics, which are distinguished by their negative Poisson's ratio, which allows them to expand in all directions during stretching[18–22]. Despite the potential benefits of the auxetics, employing the auxetics as display substrates is challenging, particularly due to their inherent perforations, which limits the use of their entire surface area[3,23,24]. Fabricating a seamless auxetic film is complicated, since filling the perforations reduces auxeticity, resulting in an increased Poisson's ratio[25,26]. Achieving an ideal substrate with a negative Poisson's ratio necessitates maximizing the difference in elastic modulus difference between the stretchable and auxetic-shaped regions[26–28].

In this study, we introduce a seamless auxetic omnidirectionally stretchable substrate (S-AUX) film for a distortion-free stretchable display. The S-AUX film exhibits a negative Poisson's ratio of −1, attaining the theoretical limit for an isotropic material while

[1]Wearable Platform Materials Technology Center (WMC), KAIST, Daejeon 34141, Republic of Korea. [2]Department of Materials Science and Engineering, KAIST, Daejeon 34141, Republic of Korea. [3]Department of Nano-Devices and Displays, Korea Institute of Machinery & Materials (KIMM) 156, Gajeongbuk-ro, Yuseong-gu, Daejeon 34103, Republic of Korea. [4]Department of Mechanical Engineering, KAIST, Daejeon 34141, Republic of Korea. [5]Department of Materials Science and Engineering, Yonsei University, Seoul 03722, Republic of Korea. [6]Department of Neurosurgery, Yonsei University College of Medicine, Seoul 03722, Republic of Korea. [7]These authors contributed equally: Yung Lee, Bongkyun Jang. e-mail: bsbae@kaist.ac.kr

maintaining a continuous, unperforated surface[29,30]. This result is facilitated by a substantial difference in moduli between two domains: (i) a glass-fabric reinforced poly(dimethylsiloxane) (PDMS) film (GFRPDMS), which forms a rigid auxetic domain, and (ii) a soft elastomer, optimized as a stretchable domain. Notably, the distinct mechanical properties of the two domains do not lead to delamination, owing to robust chemical crosslinking of silicone elastomers in both domains, which ensures the film's durability and reliability[31–33]. We explore the effects of varying differences in moduli and the films' thickness on the films' negative Poisson's ratio using various glass-fabric types and elastomer compositions. This achievement is validated through non-destructive experimental measurements, the digital image correlation method (DIC), and finite element analysis (FEA). We then integrate the S-AUX film with micro-LED arrays with a 25 pixels-per-inch (PPI) resolution, and successfully demonstrated stretchable displays with distortion-free images. Employing liquid metal electrodes with a minimum line width of 10 μm for stretchable interconnections between the micro-LED chips, the fabricated distortion-free displays sustain a 25% stretch without performance degradation, or mechanical damage.

Results

Design of S-AUX film for image distortion-free display

The schematic illustrations of an S-AUX film-based distortion-free stretchable display are depicted in Fig. 1. The in-plane omnidirectional stretchability of the S-AUX film that originates from its negative Poisson's ratio leads to a distortion-free image when stretched, contrary to the severely distorted image of a conventional elastomeric substrate with positive Poisson's ratio (Fig. 1a). The continuous and seamless surface of this S-AUX film enables the use of its full area for two-dimensional circuit fabrication. In addition, this film retains its integrated behavior under substantial mechanical deformations, unlike the traditional auxetics with perforations that show discreteness (Supplementary Fig. 1). The negative Poisson's ratio of our film results from the omnidirectional expansion of the rigid domain, leading to stretching of the stretchable domain (Fig. 1c, Supplementary Fig. 2)[34–36].

Figure 1b illustrates the S-AUX film composed of two main components. In the core, there is an auxetic-shaped GFRPDMS film, where the PDMS is reinforced by glass-fabric to provide a sufficiently high modulus. The other component is a soft low modulus silicone elastomer that fills the perforations and covers the auxetic-structured GFRPDMS film, providing a seamless and smooth surface. We employed a 'rotating square unit' type auxetic structure, which provides a sufficiently large portion of rigid area, suitable for the substrate (Supplementary Note 1)[37]. Figure 1c shows that the rigid auxetic domain induces vertical expansion during lateral stretching, through the translational and rotational motions of the square-shaped islands connected with hinges. While the stretchable domains aligned in both directions (i.e., perforations in the auxetic structure filled with soft elastomer) stretch, the seamless surface remains intact.

Fabrication of the S-AUX film consists of several steps, including the formation of the rigid domain and filling the stretchable domains (Supplementary Fig. 3). Briefly, the rigid GFRPDMS composed of glass-fabric and PDMS matrix (Sylgard 184™, Dow Corning; mixing ratio of part A:B = 10:1 unless otherwise mentioned) is patterned as an auxetic structure (Supplementary Fig. 4 and Supplementary Table 1). Subsequently, the perforations are filled with a soft silicone elastomer (Supplementary Fig. 5). The resulting S-AUX film has a continuous surface, with seamless interfaces between the glass-fabric and matrix, GFRPDMS and silicone elastomer, without any voids or pores, due to the chemical hybridization between siloxane bonds (Fig. 1d)[28].

The extent of negative Poisson's effect (i.e., auxeticity) of the S-AUX film is highly dependent on the moduli of the rigid and stretchable domains[26]. We aimed to identify the optimal differences in the moduli between the two domains that would produce both the higher auxeticity (i.e., a more negative Poisson's ratio value) and stretchability, for application in an effective image distortion-free display system. Figure 1e summarizes the tensile stress-strain curves of the materials used for the rigid and stretchable domains (details appear in Supplementary Fig. 6 and Supplementary Table 2). The GFRPDMS films (Supplementary Fig. 7) showed increasing modulus as the weaving density of the stiff glass fibers was increased, from sparse nonwoven glass-fabric to woven glass-fabric[38,39]. Specifically, the woven GFRPDMS film exhibited a significantly higher elastic modulus (E = 6.2 GPa) than the bare PDMS film (E = 0.82 MPa). Meanwhile, the modulus of the PDMS was reduced when the crosslinker content decreased. The pristine Ecoflex exhibited the lowest modulus (E = 27 kPa) and the largest elongation at a break.

Effect of material properties and geometries on Poisson's ratio

To investigate the influence of material properties and geometric dimensions on the auxeticity, we modified the composition of the rigid and stretchable domains as well as the total thickness of the S-AUX films. Here we applied an accurate image-based deformation measurement tool—the digital image correlation (DIC) analysis—for the videometric quantification of the continuous relationship between strain and Poisson's ratio. An increase in the elastic modulus of the rigid domain resulted in the transition from positive to negative Poisson's ratio. This change was due to the stiffer auxetic domains, which overcome the contraction of the stretchable domains, thereby lowering the Poisson's ratio (Fig. 2a).

Conversely, as depicted in Fig. 2b, decreasing the modulus of the stretchable domains further enhanced auxeticity. Notably, when employing Ecoflex as the filler material, the strain-Poisson's ratio curve mirrored the behavior of an unfilled domain, implying that a filler material with negligible modulus and exceptional elongation would not hinder the auxeticity any further. Using the optimum composition of woven GFRPDMS for the rigid domain and Ecoflex for the stretchable domain, we investigated the influences of thickness on the Poisson's ratio. (Fig. 2c). A lower thickness resulted in a positively shifted initial Poisson's ratio and rapidly diminishing auxeticity in the high strain region due to wrinkling, which interfered with the auxetic expansion (refer to Supplementary Note 2 and Supplementary Fig. 8). Figure 2d summarizes the relationship between the modulus difference ($E_{rigid}/E_{strechable}$) and the Poisson's ratio. The initial Poisson's ratio decreases as the modulus difference grows, due to the reduced contribution of the elastomeric stretchable domain and its high Poisson's ratio (comprehensive data available in Supplementary Table 3). When the modulus difference reaches a magnitude of five orders, the Poisson's ratio asymptotically approaches the theoretical lower limit of −1 (Supplementary Fig. 9)[40].

Remarkably, the S-AUX film that incorporated woven GFRPDMS with an Ecoflex filling ($E_{rigid}/E_{stretchable} = 2.3 \times 10^5$) exhibited the lowest Poisson's ratio of −0.99 and the highest stretchability ($\varepsilon > 23\%$). These values were attributed to the low modulus and high toughness of the Ecoflex (Supplementary Movie 1).

For a better understanding of the shape of the Poisson's ratio curve in Fig. 2d, we studied the stress-strain behavior of an S-AUX film (Fig. 2e). The curve's shape was similar to the Poisson's ratio-strain curves. The increasing modulus in phase I-II is the general behavior of a rotating square type of auxetic, which has an effective modulus, $E^* \propto [1/(1\text{-}\sin\theta)]$, where the θ represents the rotating angle of the square-shaped rigid domain[37,41]. As the film is stretched, the stretchable domain acquires amplified strain. When the restoring force of the elastomer in the stretchable domain exceeds the stiffness of the auxetic domain, the Phase III begins. The film tends to wrinkle to reduce the transversal stresses, and the Poisson's ratio steeply increases. As the elongation of the elastomer in the stretchable domain reaches its ultimate value, it starts to collapse, and stresses are

https://doi.org/10.1038/s41467-024-51516-1

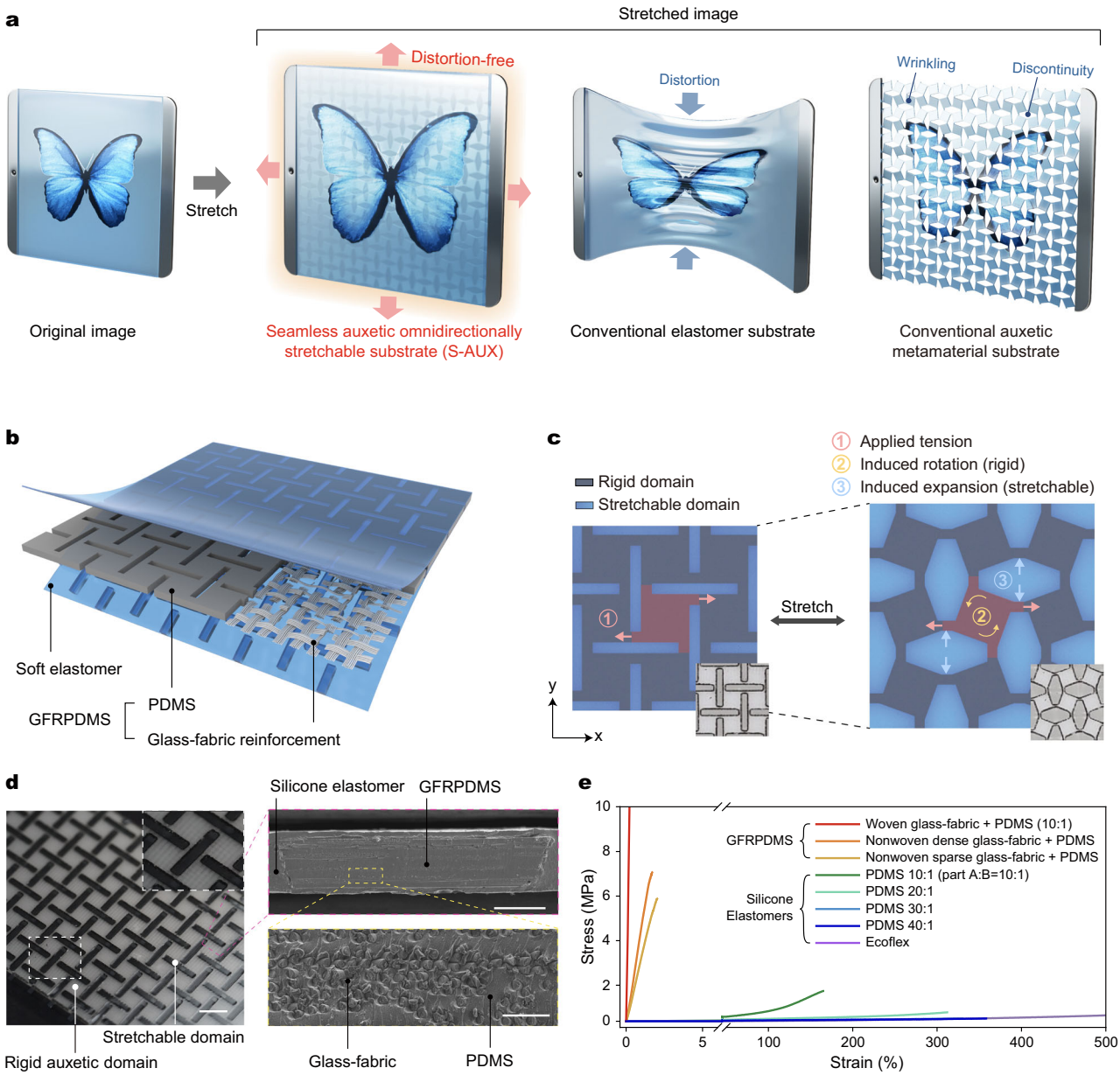

Fig. 1 | Fabrication and optimization of S-AUX film. a Schematic illustrations of stretchable displays in an original state (left), and stretched states with various substrate materials: S-AUX film (center left), conventional elastomer (center right), and conventional auxetic film (right). **b** Exploded view of S-AUX film composed of auxetic-shaped GFRPDMS and soft elastomer. **c** Operating mechanism and configurations of the S-AUX film: before stretching and stretched configuration. **d** Photographic images of the S-AUX film. A rigid auxetic domain composed of GFRPDMS has an opaque white color, while the elastomer filling the stretchable domain is transparent; Inset image shows a zoomed-in view. Scale bar, 1 mm; SEM image of the film cross-section (Scale bar, 200 μm), and magnified view (Scale bar, 20 μm). **e** Tensile stress-strain curves of the GFRPDMS films (PDMS 10:1 reinforced by various types of glass-fabric) and elastomers (PDMS and Ecoflex). Lower modulus and higher stretchability were obtained by reducing the crosslinker contents (i.e., part B) of the PDMS[46].

concentrated in the hinges of the rigid auxetic domain (phase III). However, the delamination between the two domains does not occur thanks to their strong interfacial compatibility.

Considering these results, it would be most favorable to utilize the S-AUX film within phase I-II for its highest reliability. Under a 15% cyclic stretching test, the S-AUX film exhibited superior reliability with little loss of Poisson's ratio, maintaining its initial resistance and morphology up to 5000 cycles. (Supplementary Figs. 10, 11).

Deformation behavior of S-AUX film

To investigate changes in the strain distribution within the S-AUX films under tension, we conducted a full-field digital image correlation (DIC) analysis. This technique enables the visualization of strain distribution, as depicted in Fig. 3a and Supplementary Movie 2. When the film is stretched in the vertical direction, it simultaneously expands in the transverse direction, revealing its negative Poisson's ratio, even with minimal tension. As the film elongates, the strain is concentrated in the stretchable domain ($\varepsilon_{\text{stretchable}} \cong 200\%$ at 21% loading strain). In contrast, the rigid domains remain unstretched ($\varepsilon_{\text{stretchable}} \leq 3\%$ at 21% loading strain), establishing strain-free zones where strain-sensitive devices are placed.

The results of the numerical simulation using the finite element method (FEM) validated the auxetic behavior of the S-AUX, which is induced by the differences in moduli between its two domains (Fig. 3b and Supplementary Movie 3). They also indicated a negative Poisson's effect, characterized by the rotation of the rigid auxetic domains and

https://doi.org/10.1038/s41467-024-51516-1

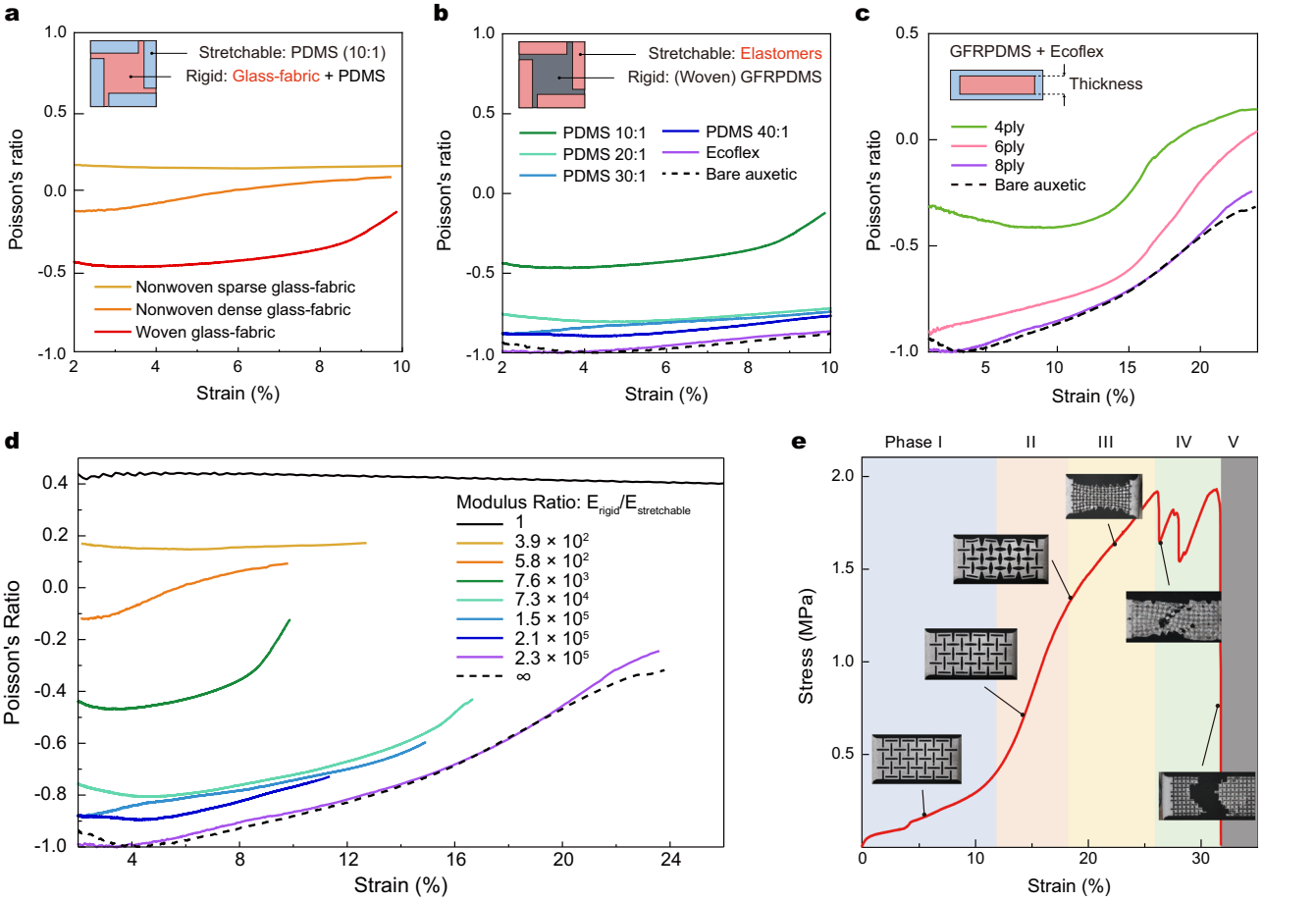

Fig. 2 | Mechanical behaviors of the S-AUX films. a–c Relative change in Poisson's ratio of S-AUX films under uniaxial tensile strain according to: (**a**) Types of glass-fabric reinforcements in GFRPDMS films, which form the rigid domain and are filled with PDMS 10:1; (**b**) Types of silicone elastomers used to fill the perforations in the auxetic structured woven GFRPDMS film; (**c**) Ecoflex-filled woven GFRPDMS films with 4, 6, and 8 layers of glass-fabrics, yielding total thicknesses of 100, 150, and 200 μm, respectively (**c**). **d** Relative change in Poisson's ratio with uniaxial tensile strain for various differences in moduli between the rigid and soft elastic domains ($E_{rigid}/E_{stretchable}$). The graph ends at the point of any fracture in any part of the film. **e** Stress-strain curve of an S-AUX film, illustrating five phases characterized by distinct slopes. Inset images depict the configurations of the film during each phase or at transition points.

the extension of the stretchable domains. At a loading strain of 21%, the glass-fabric reinforced film exhibited a maximum strain of 32%, while that of the soft elastomer reached 142%. When compared to the DIC results above, these values tend to overestimate the actual strain in the rigid domains. This disparity in their values, especially in the high-strain regions, is attributed to the out-of-plane motion of the S-AUX film and to the simplified numerical model, which does not account for all nonlinearities.

To evaluate the deformability of the S-AUX film and its capability to suppress image distortions, we conducted experiments under diverse morphing conditions. The configuration changes in the pristine PDMS (Fig. 3b) and the S-AUX film (Fig. 3c) under biaxial stretching conditions confirmed their respective distorted and distortion-free behaviors. Upon stretching, the for edges of the pristine elastomer changed into a concave shape due to its high positive Poisson's ratio. In contrast, the S-AUX film maintained its shape without any distortion, attributed to its high auxeticity. In the DIC strain map, the pristine PDMS film showed localized strain near the four grips (Supplementary Fig. 12a). On the other hand, the S-AUX film displayed uniform and omnidirectional expansion, including off-axis directions, because the deformation was induced in an auxetic structure with interconnected hinges between rigid domains.

To quantify the extent of the omnidirectional expansion, we introduced a parameter called the 'induced strain ratio'. This value is defined as the ratio of the induced diagonal shrinkage to the applied biaxial strains (Supplementary Fig. 12b). Throughout all strain ranges, the S-AUX film consistently exhibited an induced strain ratio of over 70%, showcasing its omnidirectional expansion and reduced shape distortion. In contrast, the pristine elastomer film exhibited nearly zero induced strain ratio.

We further investigated the behavior of the S-AUX film under various deformation conditions (Supplementary Fig. 13). The film displayed excellent conformity under low-radius folding, twisting, small-diameter wrapping, and poking, highlighting its versatile potential as a stretchable substrate. In conclusion, the results for the S-AUX film confirmed its excellent stretchability, reliability, and uniform deformation, making it ideal for the substrate of stretchable display.

Image distortion-free display application

Utilizing the outstanding image distortion inhibition capabilities of the S-AUX film, we fabricated a high-resolution stretchable display on the S-AUX film by incorporating a 25 PPI micro-LED array and liquid metal interconnections (Fig. 4a). The fabrication process involved a straightforward transferring of the micro-LED array onto the rigid auxetic domain of the S-AUX film using the roll transfer method (Supplementary Fig. 14a). Subsequently, liquid metal electrodes were directly printed to interconnect the contact electrode pads of the micro-LEDs (Supplementary Fig. 14b). Thanks to the seamless surface of the S-AUX film, the circuit configuration could be greatly simplified. The precise liquid metal

https://doi.org/10.1038/s41467-024-51516-1

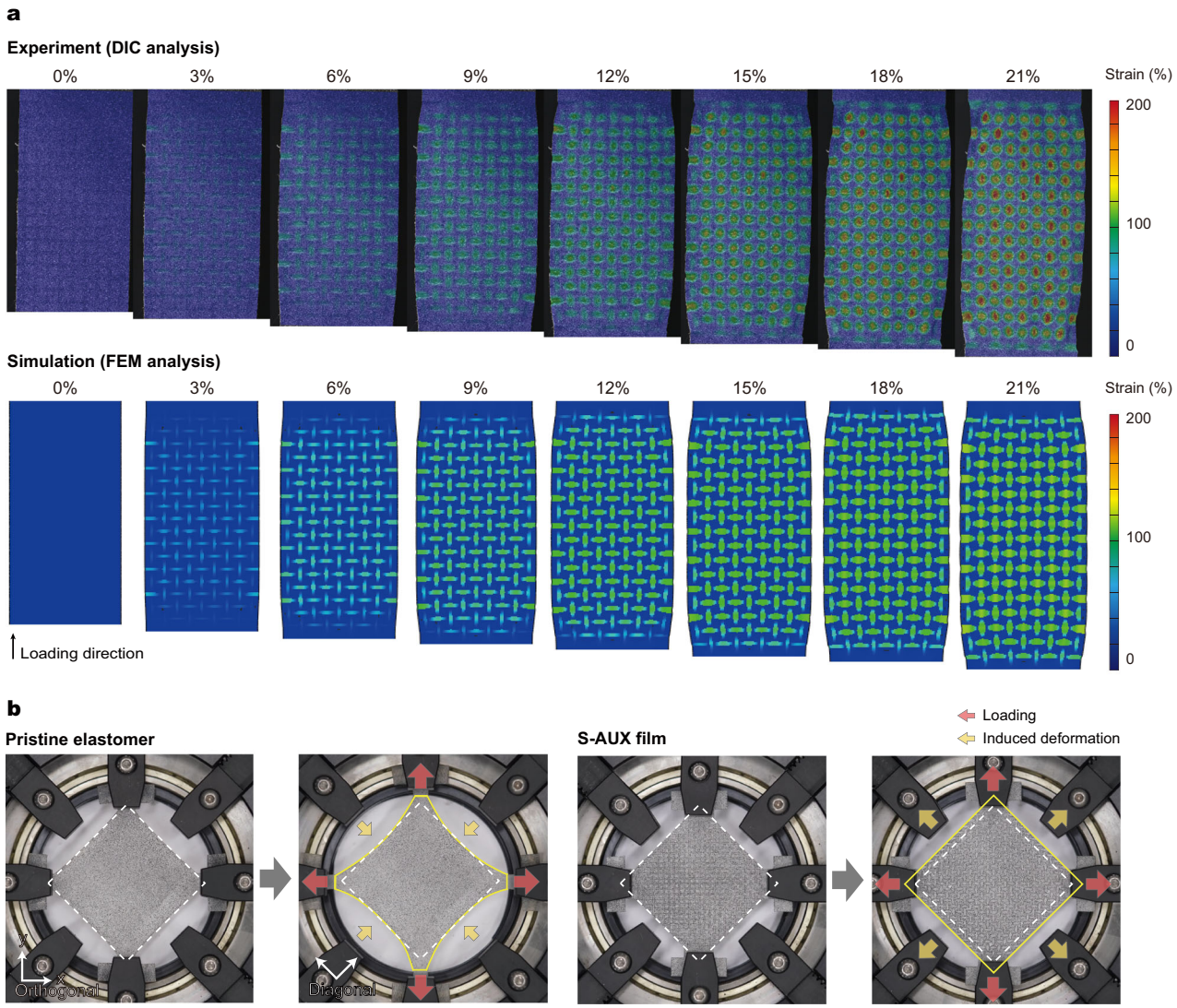

Fig. 3 | Theoretical Comparison and Distortion reduction ability. **a** Configurations and visualized principal strain distribution of the optimized S-AUX film at various strain rates: Experimental results were obtained using the digital image correlation (DIC) method; In-plane principal strain distribution within the S-AUX film, obtained by a numerical simulation using FEM. The load was applied in the vertical direction (x-axis), which resulted in transversal displacement (y-axis) due to the negative Poisson's ratio. **b** Configuration change in the pristine elastomer and the S-AUX film under biaxial stretching. (red arrows: applied stretching, and yellow arrows: induced deformation).

printing method, with a minimum linewidth of 10 μm, enabled an elaborate circuit to be fabricated for this high-resolution micro-LED display (Fig. 4b). The adoption of a two-step linewidth fabrication strategy further ensured the stable and reliable driving of the devices.

The S-AUX film-based stretchable display has a distortion-free stretching characteristic owing to the auxetic behavior (Fig. 4c). The heart-shaped image retained its shape reversibly during uniaxial stretching and releasing (Supplementary Fig. 15 and Supplementary Movies 4, 5). When subjected to transversal loading, the display not only maintained a uniform shape but also showed consistent driving performances without any loss on light intensity up to 20% strain (Fig. 4d and Supplementary Fig. 16). During the stretching, each micro-LED on rigid strain-free domain only rotated while the liquid metal electrodes crossing the stretchable area were elongated.

To evaluate the stability of the stretchable display, I-V curves were measured at various stretch levels (Fig. 4e). The consistent IV curves across strains of up to 20% confirmed its excellent stability. Furthermore, the display exhibited stable light emission up to 20–25% stretching (Supplementary Figs. 17, 18 and Supplementary Movie 6). We also confirmed the resilience of the stretchable display under cyclic stretching at 15% strain (Fig. 4f, Supplementary Fig. 19 and Supplementary Movie 7). Remarkably, even after 300 cycles of stretching and recovery, the device retained its original resistance and light-emitting functionalities. These exceptional performances and reliability are attributed to the stable functionality of the S-AUX film and the excellent stretchability of the liquid metal electrodes.

Discussion

In summary, our work culminated in the development of a seamless auxetic omnidirectionally stretchable substrate (S-AUX) film that achieved an optimal negative Poisson's ratio of −1. This was accomplished by maximizing the difference in moduli between the rigid and stretchable domains. By integrating a robust glass-fabric reinforcement and PDMS we significantly increased the modulus of the auxetic-structured rigid domains. A seamless surface was achieved by filling the perforations in the rigid auxetic domains with a low-modulus elastomer that was highly compatible with the PDMS matrix of the rigid domain. The resulting film exhibited exceptional characteristics: it effectively inhibits image distortion, offers free deformability, and allows for full-area utilization as a stretchable

https://doi.org/10.1038/s41467-024-51516-1

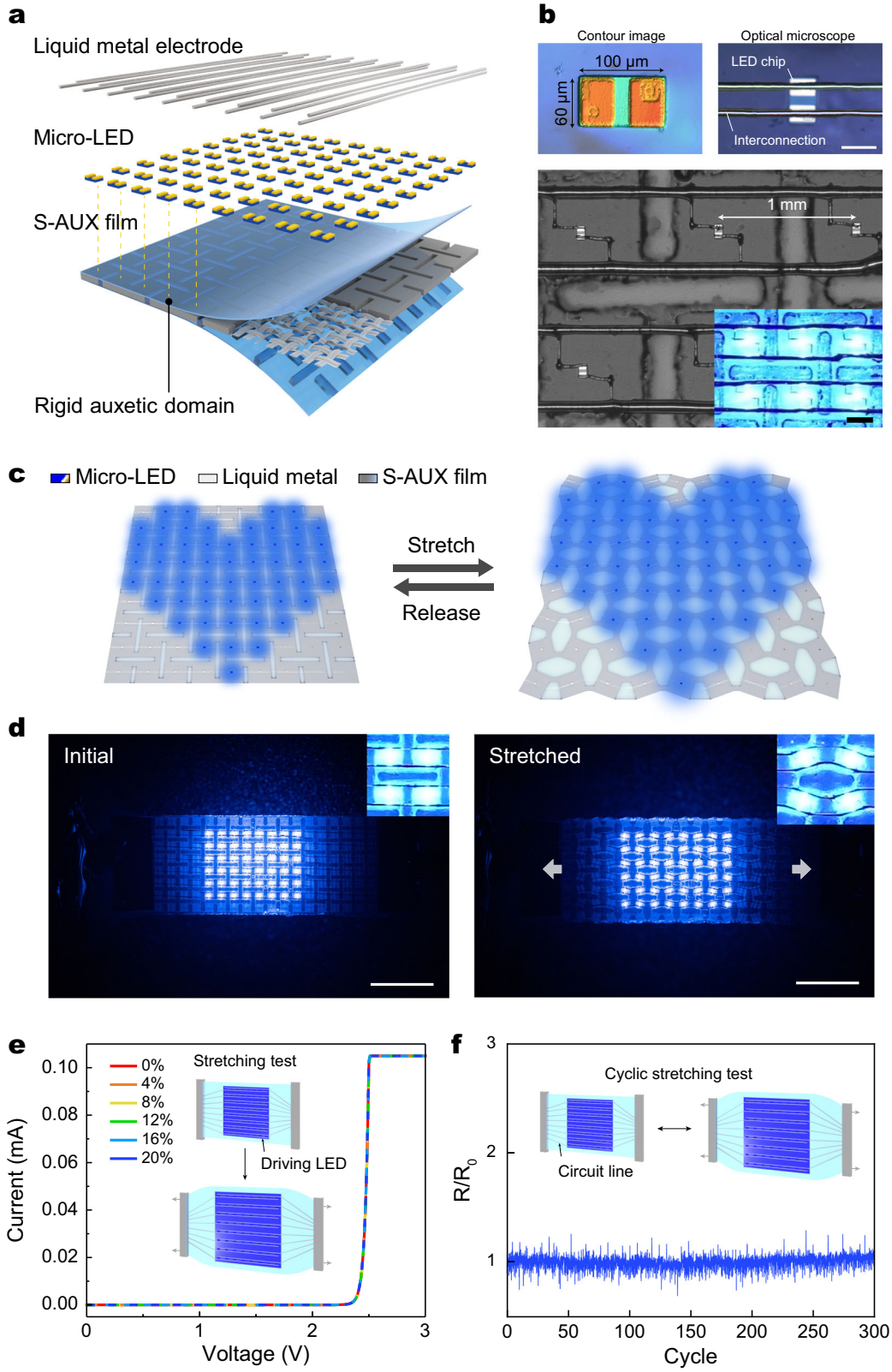

substrate. The straightforward roll micro-LED transfer technique and greatly simplified interconnections formed by the direct liquid metal printing method enabled the fabrication of highly reliable, high-resolution stretchable displays (Supplementary Tables 4-5). The film's unique seamless surface and omnidirectionally stretchable nature offer significant advances in the field of stretchable electronics, for applications across a wide spectrum including displays, wearable electronics, healthcare devices, sensors, batteries, energy conversion devices, soft robotics, and human-machine interfaces.

Methods

Fabrication of the S-AUX films

Fabrication of the S-AUX films was carried out in five steps.

Fig. 4 | Demonstration of the distortion-free S-AUX film-based stretchable display. a Structural configuration of the distortion-free display components on the S-AUX film. Micro LEDs were placed on each square island of the rigid auxetic domain. Liquid metal electrodes were directly printed for interconnections. **b** Contour image of a micro-LED chip transferred onto the S-AUX film: emissive layer (green) and contact electrodes (orange) Scale bar= 50 μm; optical microscope images of a micro-LED chip on the S-AUX film, with 10 μm-thick liquid metal interconnections Scale bar= 50 μm; micro-LED array with a pitch distance of 1 mm and liquid metal interconnections with another configuration Scale bar= 200 μm, and its light-on state (inset). **c** Schematic illustrations of the S-AUX film-based image distortion-free display in its stretched state and released state. **d** Photographic images of the S-AUX film-based display: released state and stretched state. Scale bars= 5 mm. **e** I-V curves under uniaxial stretching from 0% to 20%, respectively. **f** Cyclic stretching reliability of the distortion-free display under repeated strain of 15% for 300 times. Plot is the normalized resistance change during cyclic stretching.

i) Fabrication of a glass-fabric reinforced elastomer film. Layers of 25 μm thick glass-fabrics (E-glass #1037, Nittobo. Weaving density: 69 (warp) × 72 (weft) per square inch) were placed on a hydrophobic surface-treated carrier glass. Subsequently, a PDMS (Sylgard 184™, part A:B = 10:1) premixture solution was poured on the glass-fabric. The glass-fabric reinforced elastomer film was fabricated using a vacuum bag lamination process at room temperature, followed by room temperature vulcanization of a silicone elastomer matrix[38,42].

ii) Patterning auxetic structure. The glass-fabric reinforced elastomer film was patterned as an auxetic structure using a CO_2 laser cutter (LP-400 series; Panasonic). The laser power and scan speed were modulated to obtain the finest cut. For facile measurements of the strain and Poisson's ratio under uniaxial tension, a dog-bone type specimen was prepared. The detailed dimensions of the structures followed the values listed in Supplementary Table 1. To fabricate the stretchable display, specimens were fabricated with proportionally reduced dimensions to obtain a rigid domain with smaller sizes and pitches (Specimen number 2 in Supplementary Table 1).

iii) Filling the perforations of the auxetic structured glass-fabric reinforced elastomer film. The laser-patterned film was impregnated into another silicone elastomer premixture resin. To form a solid interface, the glass-fabric reinforced film was treated with O_2 plasma before impregnation. To optimize the modulus differences, Ecoflex (Ecoflex 00-30™, part A:B = 1:1 mixing ratio; Smooth-on) and PDMS with various cross-linker contents (i.e., part B) contents from A:B = 10:1 to 40:1 were used. For optimal S-AUX film composition, Ecoflex was used.

iv) Forming a flat surface. The impregnated glass-fabric reinforced elastomer film was placed between and covered by surface-treated glasses. The film was cured at room temperature until it was fully cured.

Mechanical characterization

Tensile testing of each material was conducted using a universal tensile machine (AGS-X, Shimadzu, Japan). Dog-bone type tensile testing specimens were prepared via CO_2 laser cutting to have a gauge width of 3 mm and gauge length of 45 mm (Supplementary Fig. 1). The extension speed was set to 45 mm/min.

Digital Image Correlation (DIC) analysis

Matte white and black sprays were applied to the specimens to obtain uniform but irregular speckle patterns for full-field strain analysis. The specimens were installed in the tensile testing machine for stretching, then movies were taken during the stretching using a CMOS (complementary metal oxide semiconductor) sensor digital camera (a7c, Sony) with 30 fps. The images from the movie were separated frame by frame and analyzed using a commercial DIC software (Aramis, GOM GmbH).

Poisson's ratio measurement

Dog bone-type specimens were used for the Poisson's ratio measurement. To track the change in length, fiducial points for the x- and y-axes were respectively marked on the end-center of the neck of dog bone specimens using a marker pen. (Supplementary Fig. 20) A movie taken during the uniaxial stretching of each specimen was processed frame by frame using digital image correlation (DIC) software (Aramis professional, GOM GmbH). The axial strains were defined as the length change ΔL with respect to the original length L of the initial state: $(\Delta L/L)\times 100$. The Poisson's ratio (ν) was then calculated using the obtained y-axis strain (ε_y) and x-axis strain (ε_x) data as: $\nu = -\varepsilon_y/\varepsilon_x$. The Poisson's ratio value measured from the initial state to 2% of applied strain (ε_x) was ignored due to the high error levels.

Finite element method (FEM) simulation

A finite element analysis (FEA) of the S-AUX film was conducted to investigate the effect of a negative Poisson's ratio under unidirectional tension. The material properties of the pristine cover elastomer were determined by fitting the results from uniaxial tension tests of Ecoflex to the Arruda-Boyce hyper-elastic material model, while the auxetic reinforced domain was assumed to be a linear elastic material ($E = 6.2$ GPa and $\nu = 0.1$). The strain distribution and Poisson's ratio of the dog bone-shaped S-AUX film under tensile loading were evaluated using the commercial finite-element method (FEM) solver ABAQUS.

Transfer of micro-LED arrays

Flip chip micro-LEDs were fabricated based on gallium nitride (GaN) epitaxy layers on a 4-inch sapphire wafer via deposition and patterning processes. The micro-LEDs were then rearranged on the temporary substrate before transferring. Subsequently, the array of micro-LEDs was transferred onto the S-AUX film using a PDMS roll stamp equipped in a roll transfer machine (Supplementary Fig. 14a)[43]. Here, an S-AUX film covered with an optically clear adhesive in advance. The roll transfer process used optical microscopes to ensure precise alignment of the micro-LED array at the center of the rigid domain in the auxetic pattern.

Fabrication of liquid metal interconnections

To fabricate the liquid metal interconnections, we used a direct printing system (Supplementary Fig. 14b)[44,45]. This system consists of a nozzle connected to an ink reservoir, a pneumatic pressure controller, and a 6-axis stage. To prepare different diameter nozzles, we used a pipette puller to make a glass capillary with an inner diameter of 30 μm, as well as conventional metal nozzles with inner diameters of 100 μm. The nozzle was then connected to an ink reservoir containing a liquid metal (EGaIn, 75.5% Ga and 24.5% In alloy by weight, Changsha Santech Materials Co. Ltd.), and a substrate was placed on the 6-axis stage. All the printing steps were monitored using a microscope camera (QImaging Micropublisher 5.0 RTV, Teledyne Photometrics) to ensure precise micro-movements. The printing methods were divided into two consecutive steps. First, for the electrical interconnection of each micro-LED array, we used a glass capillary-based nozzle to print a linewidth of 30 μm within the metal pads of the micro-LED. Then, a linewidth ranging from 70 to 80 μm was printed using a metal-based nozzle to connect each interconnection with the positive and negative terminals, enabling power to be delivered to the micro-LED arrays.

Data availability

The authors declare that all data supporting the findings of this study are available within the paper and its supplementary information files. The rest of the data are available from the corresponding author upon request.

References

1. Wang, J. X. & Lee, P. S. Progress and Prospects in Stretchable Electroluminescent Devices. *Nanophotonics* **6**, 435–451 (2017).
2. Yin, D. et al. Efficient and mechanically robust stretchable organic light-emitting devices by a laser-programmable buckling process. *Nat. Commun.* **7**, 11573 (2016).
3. Koo, J. H. et al. A vacuum-deposited polymer dielectric for wafer-scale stretchable electronics. *Nat. Electron.* **6**, 137–145 (2023).
4. Choi, D. K. et al. Highly efficient, heat dissipating, stretchable organic light-emitting diodes based on a MoO3/Au/MoO3 electrode with encapsulation. *Nat. Commun.* **12**, 2864 (2021).
5. Liang, J. J., Li, L., Niu, X. F., Yu, Z. B. & Pei, Q. B. Elastomeric polymer light-emitting devices and displays. *Nat. Photonics* **7**, 817–824 (2013).
6. Sekitani, T. et al. Stretchable active-matrix organic light-emitting diode display using printable elastic conductors. *Nat. Mater.* **8**, 494–499 (2009).
7. Morikawa, Y. et al. Ultrastretchable Kirigami Bioprobes. *Adv. Healthc. Mater.* **7**, 1701100 (2018).
8. Won, P. et al. Stretchable and Transparent Kirigami Conductor of Nanowire Percolation Network for Electronic Skin Applications. *Nano Lett.* **19**, 6087–6096 (2019).
9. Hu, X. L. et al. Stretchable Inorganic-Semiconductor Electronic Systems. *Adv. Mater.* **23**, 2933–2936 (2011).
10. Kim, D. H. et al. Epidermal Electronics. *Science* **333**, 838–843 (2011).
11. Jang, K. I. et al. Rugged and breathable forms of stretchable electronics with adherent composite substrates for transcutaneous monitoring. *Nat. Commun.* **5**, 4779 (2014).
12. Kim, R. H. et al. Waterproof AlInGaP optoelectronics on stretchable substrates with applications in biomedicine and robotics. *Nat. Mater.* **9**, 929–937 (2010).
13. Kim, D. H. et al. Stretchable and foldable silicon integrated circuits. *Science* **320**, 507–511 (2008).
14. Yokota, T. et al. Ultraflexible organic photonic skin. *Sci. Adv.* **2**, e1501856 (2016).
15. Park, S. I. et al. Printed Assemblies of Inorganic Light-Emitting Diodes for Deformable and Semitransparent Displays. *Science* **325**, 977–981 (2009).
16. Jang, B. et al. Auxetic Meta-Display: Stretchable Display without Image Distortion. *Adv. Funct. Mater.* **32**, 2113299 (2022).
17. Yu, Z. B., Niu, X. F., Liu, Z. T. & Pei, Q. B. Intrinsically Stretchable Polymer Light-Emitting Devices Using Carbon Nanotube-Polymer Composite Electrodes. *Adv. Mater.* **23**, 3989 (2011).
18. Slann, A., White, W., Scarpa, F., Boba, K. & Farrow, I. Cellular plates with auxetic rectangular perforations. *Phys. Status Solidi B-Basic Solid State Phys.* **252**, 1533–1539 (2015).
19. Choi, G. P. T., Dudte, L. H. & Mahadevan, L. Programming shape using kirigami tessellations. *Nat. Mater.* **18**, 999 (2019).
20. Lakes, R. Foam Structures with a Negative Poissons Ratio. *Science* **235**, 1038–1040 (1987).
21. Lipton, J. I. et al. Handedness in shearing auxetics creates rigid and compliant structures. *Science* **360**, 632–635 (2018).
22. Greaves, G. N., Greer, A. L., Lakes, R. S. & Rouxel, T. Poisson's ratio and modern materials. *Nat. Mater.* **10**, 823–837 (2011).
23. Overvelde, J. T. B., Shan, S. & Bertoldi, K. Compaction Through Buckling in 2D Periodic, Soft and Porous Structures: Effect of Pore Shape. *Adv. Mater.* **24**, 2337–2342 (2012).
24. Rao, Z. Y. et al. Curvy, shape-adaptive imagers based on printed optoelectronic pixels with a kirigami design. *Nat. Electron.* **4**, 513–521 (2021).
25. Zied, K. & AL-Grafi, M. Design of auxetic sandwich panel faceplates comprising cellular networks with high stiffness and negative Poisson's ratio. *Adv. Compos Mater.* **24**, 175–196 (2015).
26. Pozniak, A. A., Wojciechowski, K. W., Grima, J. N. & Mizzi, L. Planar auxeticity from elliptic inclusions. *Compos Part B-Eng.* **94**, 379–388 (2016).
27. Peng, X. L., Soyarslan, C. & Bargmann, S. Phase contrast mediated switch of auxetic mechanism in composites of infilled re-entrant honeycomb microstructures. *Extreme Mech. Lett.* **35**, 100641 (2020).
28. Wang, W. C. et al. Strain-insensitive intrinsically stretchable transistors and circuits. *Nat. Electron.* **4**, 143–150 (2021).
29. Grima, J. N., Alderson, A. & Evans, K. E. Auxetic behaviour from, rotating rigid units. *Phys. Status Solidi B-Basic Solid State Phys.* **242**, 561–575 (2005).
30. Suzuki, Y. et al. Self-assembly of coherently dynamic, auxetic, two-dimensional protein crystals. *Nature* **533**, 369 (2016).
31. Qi, D. P., Zhang, K. Y., Tian, G. W., Jiang, B. & Huang, Y. D. Stretchable Electronics Based on PDMS Substrates. *Adv. Mater.* **33**, 2003155 (2021).
32. Yun, K. S. & Yoon, E. Fabrication of complex multilevel microchannels in PDMS by using three-dimensional photoresist masters. *Lab a Chip* **8**, 245–250 (2008).
33. Tan, P. et al. Solution-processable, soft, self-adhesive, and conductive polymer composites for soft electronics. *Nat. Commun.* **13**, 358 (2022).
34. Grima, J. N., Mizzi, L., Azzopardi, K. M. & Gatt, R. Auxetic Perforated Mechanical Metamaterials with Randomly Oriented Cuts. *Adv. Mater.* **28**, 385–389 (2016).
35. Mizzi, L., Grima, J. N., Gatt, R. & Attard, D. Analysis of the Deformation Behavior and Mechanical Properties of Slit-Perforated Auxetic Metamaterials. *Phys. Status Solidi B-Basic Solid State Phys.* **256**, 180153 (2019).
36. Kim, M. S. et al. Skin-like Omnidirectional Stretchable Platform with Negative Poisson's Ratio for Wearable Strain-Pressure Simultaneous Sensor. *Adv. Funct. Mater.* **33**, 2208792 (2023).
37. Grima, J. N. & Evans, K. E. Auxetic behavior from rotating squares. *J. Mater. Sci. Lett.* **19**, 1563–1565 (2000).
38. Lee, Y. et al. Transparent and flexible hybrid cover window film: Hard coating/substrate all-in-one composite film for reliable foldable display. *Composites Part B-Engineering* **247**, 110336 (2022).
39. Jang, J., Im, H. G., Lim, D. & Bae, B. S. Preparation of high-performance transparent glass-fiber reinforced composites based on refractive index-tunable epoxy-functionalized siloxane hybrid matrix. *Composites Sci. Technol.* **201**, 108521 (2021).
40. Bertoldi, K., Reis, P. M., Willshaw, S. & Mullin, T. Negative Poisson's Ratio Behavior Induced by an Elastic Instability. *Adv. Mater.* **22**, 361-366 (2010).
41. Grima, J. N., Farrugia, P. S., Caruana, C., Gatt, R. & Attard, D. Auxetic behaviour from stretching connected squares. *J. Mater. Sci.* **43**, 5962–5971 (2008).
42. Wallin, T. J. et al. 3D printable tough silicone double networks. *Nat. Commun.* **11**, 4000 (2020).
43. Choi, M. et al. Stretchable Active Matrix Inorganic Light-Emitting Diode Display Enabled by Overlay-Aligned Roll-Transfer Printing. *Adv. Funct. Mater.* **27**, 1606005 (2017).
44. An, H. S. et al. High-Resolution 3D Printing of Freeform, Transparent Displays in Ambient Air. *Adv. Sci.* **6**, 1901603 (2019).
45. Park, Y. G., An, H. S., Kim, J. Y. & Park, J. U. High-resolution, reconfigurable printing of liquid metals with three-dimensional structures. *Sci. Adv.* **5**, eaaw2844 (2019).
46. Trappmann, B. et al. Extracellular-matrix tethering regulates stem-cell fate. *Nat. Mater.* **11**, 642–649 (2012).

Acknowledgements

This work was supported by the Wearable Platform Materials Technology Center (WMC) supported by a National Research Foundation of Korea (NRF) Grant funded by the Korean Government (MSIT) (NRF-2022R1A5A6000846). This work was also supported by an internal research program of the Korea Institute of Machinery and Materials

(NK248C). This work was also supported by the LG Display (C2023005309_v1).

Author contributions

Y.L. and B.-S.B. designed the project and experiments. Y.L. fabricated and characterized the seamless auxetic substrate films. Y.L., B.K.J., H.S.K., and J.-H.K. fabricated micro-LED stretchable devices and analyzed data with contributions from all authors. H.S. and T.-S.K. carried out mechanical simulations. S.K., Y.W.K., and J.-U.P. undertook the direct printing of liquid metal interconnections and electrical characterizations. M.S. and I.P. helped with incipient conception and mechanical characterizations. Y.L., B.K.J., J.J., J.-H.K., J.-U.P., and B.-S.B. wrote the paper. All authors reviewed and commented on the manuscript.

Competing interests

The authors declare no competing interests.

Additional information

Supplementary information The online version contains supplementary material available at https://doi.org/10.1038/s41467-024-51516-1.

Correspondence and requests for materials should be addressed to Byeong-Soo Bae.

Peer review information *Nature Communications* thanks the anonymous, reviewer(s) for their contribution to the peer review of this work. A peer review file is available.